

# Deeper Understanding of Black-box Predictions via Generalized Influence Functions

Hyeonsu Lyu<sup>1</sup>, Jonggyu Jang<sup>1</sup>, Sehyun Ryu<sup>1</sup>, Hyun Jong Yang<sup>1</sup>

<sup>1</sup> POSTECH, Korea

## Abstract

Influence functions (IFs) elucidate how learning data affects model behavior. However, growing non-convexity and the number of parameters in modern large-scale models lead to imprecise influence approximation and instability in computations. We highly suspect that the first-order approximation in large models causes such fragility, as IFs change all parameters including possibly nuisance parameters that are irrelevant to the examined data. Thus, we attempt to selectively analyze parameters associated with the data. However, simply computing influence from the chosen parameters can be misleading, as it fails to nullify the subliminal impact of unselected parameters. Our approach introduces generalized IFs, precisely estimating target parameters' influence while considering fixed parameters' effects. Unlike the classic IFs, we newly adopt a method to identify pertinent target parameters closely associated with the analyzed data. Furthermore, we tackle computational instability with a robust inverse-Hessian-vector product approximation. Remarkably, the proposed approximation algorithm guarantees convergence regardless of the network configurations. We evaluated our approach on ResNet-18 and VGG-11 for class removal and backdoor model recovery. Modifying just 10% of the network yields results comparable to the network retrained from scratch. Aligned with our first guess, we also confirm that modifying an excessive number of parameters results in a decline in network utility. We believe our proposal can become a versatile tool for model analysis across various AI domains, appealing to both specialists and general readers. Codes are available at <https://github.com/hslyu/GIF>.

## 1 Introduction

“*Fear always springs from ignorance*” by Emerson (1841) well represents the anxiety of our society on AI. Recent requests from worldwide scholars and entrepreneurs to halt the training of large language models reflect such growing concern (Anderson 2023). Over a couple of decades, astonishing technical advancements have shown the capabilities of AI, yet the extent to which AI can expand still remains unknown.

Influence functions are suggested to unveil the enigmatic black-box models (Koh and Liang 2017; Barredo Arrieta et al. 2020). Influence functions, originating from classical statistics (Hampel 1974), can describe the model’s behavior by identifying how training data contributes to the model prediction.

Diverse tasks have been solved under the realm of influence functions. For example, Lee et al. (2020); Wang et al.

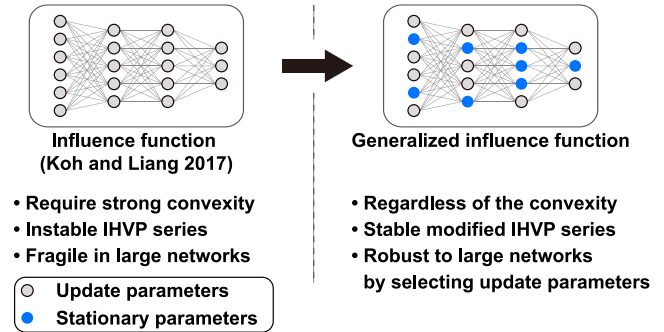


Figure 1: Summary of the difference between the influence functions (Koh and Liang 2017) and the generalized influence functions. The generalized influence functions attempt to accurately approximate only the changes in the update parameters. We also develop an inverse-hessian-vector product (IHVP) series to implement the generalized influence functions, of which convergence is mathematically guaranteed.

(2020) extended influence functions to the area of data processing; Jain et al. (2022); Ye et al. (2022); Brunet et al. (2019) applied them into natural language processing; Cohen and Giryes (2022); Koh, Steinhardt, and Liang (2022) proposed model attacking; and Kong, Shen, and Huang (2022); Schulam and Saria (2019) designed post-processing methods for trained models. In the meantime, there are consistent reports of deficiencies in influence functions, even though influence functions have demonstrated remarkable versatility and wide-ranging applicability in the literature.

Basu, Pope, and Feizi (2021); Epifano et al. (2023) found that influence functions can be susceptible to the non-convex nature of the system. The inherent fragility cannot be avoided because influence functions depend on the inverse Hessian-vector product, assuming the positive semi-definiteness of the Hessian matrix. Thus, Basu, You, and Feizi (2020); Koh et al. (2019); Bae et al. (2022) detour the problem by applying  $L_2$  regularization in the loss function. This approach serves to shift the eigenvalues of the Hessian by the regularization weight. However, applying  $L_2$  regularization is provisional, as it cannot be applicable to networks trained without  $L_2$  regularization.

Another significant hurdle is inaccuracy in large models.

To the best of our knowledge, there is no complete explanation for why the inaccuracy in estimation intensifies as the number of parameters increases, although such imprecision has been reported in prior research (Koh et al. 2019; Basu, Pope, and Feizi 2021; Epifano et al. 2023).

A suspicious candidate is the estimation error. Influence functions utilize first-order Taylor approximation to compute the alteration of the *entire* parameters. However, not all parameters are involved with a given input data group (Olah et al. 2018; Bau et al. 2020). Nuisance changes in irrelevant parameters and truncation accumulate and then may cause lossy updates, especially for large networks. In metaphor, sweeping the entire network may result in the inadvertent removal of a small brain fragment while operating knee surgery.

To resolve the challenges, we newly define generalized influence functions (GIFs) by separating the network into target and fixed parameters as in Fig. 1. The GIFs fine-tune the target parameters to render the gradients of both target and fixed parameters zero, whereas the conventional influence functions overlook the gradient components of the fixed (frozen) parameters. Remarkably, the convergence of the GIFs is mathematically guaranteed *for any given network* due to the scale-invariancy and positive-definiteness.

We guess that there are good combinations of parameters that effectively minimize the gradients for all parameters, as in the network pruning (Frankle and Carbin 2019). Thus, we suggest lightweight parameter-selection algorithms compatible with networks containing linear or convolutional layers.

These approaches provide plug-and-play influence functions for any network regardless of loss configurations. Numerical implementations show that the GIF is faster and more accurate than the conventional influence function.

## 2 Approach

### 2.1 Preliminary: Influence Function

Koh and Liang (2017) introduced an influence function, which measures the change in model parameters when the empirical risk infinitesimally changes. Consider a model with parameter  $\theta$  in the parameter space  $\Theta \subset \mathbb{R}^n$  and  $m$  training examples  $z_1, \dots, z_m \in Z$ . The empirical risk can be defined as  $\mathcal{L}(\theta) = \sum_{i=1}^m \ell(z_i, \theta)$  for some loss function  $\ell(\cdot)$ . The empirical risk minimizer  $\hat{\theta}$  is accordingly defined as  $\hat{\theta} = \operatorname{argmin}_{\theta \in \Theta} \mathcal{L}(\theta)$ .

The influence function can provide an approximated parameter change when the loss of a training example  $z$  is  $\epsilon$ -upweighted, where the new empirical risk minimizer is given by  $\hat{\theta}(\epsilon, z) = \operatorname{argmin}_{\theta \in \Theta} \mathcal{L}(\theta) + \epsilon \ell(z, \theta)$ . The influence function  $\mathcal{I}(z, \hat{\theta})$  computes the difference between the two risk minimizers  $\hat{\theta}$  and  $\hat{\theta}(\epsilon, z)$ . By using the trained parameter  $\hat{\theta}$  as an anchor, the first-order optimality condition for  $\hat{\theta}(\epsilon, z)$  can be linearly approximated (see, e.g., Koh and Liang (2017) for details) as

$$0 \approx \epsilon \nabla \ell(z, \hat{\theta}) + \mathbf{H}_{\hat{\theta}}(\hat{\theta}(\epsilon, z) - \hat{\theta}), \quad (1)$$

where  $\mathbf{H}_{\hat{\theta}} = [h_1 | \dots | h_n] = \nabla^2 \mathcal{L}(\hat{\theta}) \in \mathbb{R}^{n \times n}$ . From (1),

influence function can be defined as

$$\mathcal{I}(z, \hat{\theta}) := \frac{d(\hat{\theta}(\epsilon, z) - \hat{\theta})}{d\epsilon} = -\mathbf{H}_{\hat{\theta}}^{-1} \nabla \ell(z, \hat{\theta}). \quad (2)$$

### 2.2 Generalized Influence Function

We propose the GIF to answer the following question: *How can we measure the influence of data  $z$  on the arbitrarily chosen parameters?* Measuring the partial change in the existing regime might be infeasible because the original influence functions cannot nullify the effect of the non-zero components in  $\nabla \ell(z, \hat{\theta})$ . We suggest a separation of parameters to accurately measure the effect on the influential parameters. Specifically, we divide the parameters in  $\theta$  into two groups: i) one group for measuring the influence, and ii) the other group to be unchanged.

Let us denote parameters in the network as  $\theta_1, \dots, \theta_n$  where  $\theta = [\theta_1, \dots, \theta_n]^T$ . By using the index set  $J = \{j_1, \dots, j_k\}$  with  $k$  indexes, we define a sub-parameter  $\theta_J = [\theta_{j_1}, \dots, \theta_{j_k}]^T \in \mathbb{R}^k$  and  $\theta_{-J} = [\theta_j]_{j \notin J} \in \mathbb{R}^{n-k}$ , which indicate the target parameters and fixed parameters, respectively.

For brevity of derivations, we rearrange all terms in (1) as  $\hat{\theta} = [\hat{\theta}_J, \hat{\theta}_{-J}]^T$  and  $\mathbf{H} = [\mathbf{H}_J | \mathbf{H}_{-J}]$  for  $\mathbf{H}_J = [h_j]_{j \in J}$  and  $\mathbf{H}_{-J} = [h_i]_{i \notin J}$ . Then, (1) can be represented as

$$0 \approx \epsilon \nabla \ell(z, \hat{\theta}) + [\mathbf{H}_J | \mathbf{H}_{-J}] \left( \begin{bmatrix} \hat{\theta}_J(\epsilon, z) \\ \hat{\theta}_{-J} \end{bmatrix} - \begin{bmatrix} \hat{\theta}_J \\ \hat{\theta}_{-J} \end{bmatrix} \right). \quad (3)$$

Note that the  $\hat{\theta}_{-J}$  terms cancel each other, not affecting the equation. Thus, (1) can be rewritten as

$$0 \approx \epsilon \nabla \ell(z, \hat{\theta}) + [\mathbf{H}_J | \mathbf{H}_{-J}] \begin{bmatrix} \Delta_\epsilon \\ \mathbf{0} \end{bmatrix} \quad (4)$$

$$= \epsilon \nabla \ell(z, \hat{\theta}) + \mathbf{H}_J \Delta_\epsilon, \quad (5)$$

where  $\Delta_\epsilon = \hat{\theta}_J(\epsilon, z) - \hat{\theta}_J \in \mathbb{R}^k$ .

Finding  $\Delta_\epsilon$  in (5) is an overdetermined problem where the least-square method provides mathematical optimum. Then, the influence of data point  $z$  on  $\hat{\theta}_J$  is defined as

$$\mathcal{I}(z, \hat{\theta}_J | \hat{\theta}) := \frac{d\Delta_\epsilon}{d\epsilon} = -(\mathbf{H}_J^T \mathbf{H}_J)^{-1} \mathbf{H}_J^T \nabla \ell(z, \hat{\theta}). \quad (6)$$

The original influence function can be reproduced from (6) by setting  $J = \{1, \dots, n\}$ . Then,

$$\mathcal{I}(z, \hat{\theta} | \hat{\theta}) = \mathcal{I}(z, \hat{\theta}) = -\mathbf{H}_{\hat{\theta}}^{-1} \nabla \ell(z, \hat{\theta}), \quad (7)$$

as the Hessian  $\mathbf{H}$  is full-rank.

### 2.3 Group Effect on Influence Function

Suppose that a group of data is given to measure influence on the target parameter  $\hat{\theta}_J$ . The loss of data points in the group is  $\epsilon$ -upweighted, where the empirical risk minimizer is given by  $\hat{\theta}(\epsilon, \mathbf{w}) = \operatorname{argmin}_{\theta \in \Theta} \mathcal{L}(\theta) + \epsilon \sum_{i=1}^m w_i \ell(z_i, \theta)$ , where  $\mathbf{w} = [w_1, \dots, w_m]^T \in \{0, 1\}^m$  indicates whether each training example is upweighted or not<sup>1</sup>.

<sup>1</sup>GIF (6) can be generalized by setting  $\mathbf{w}$  as a one-hot vector.

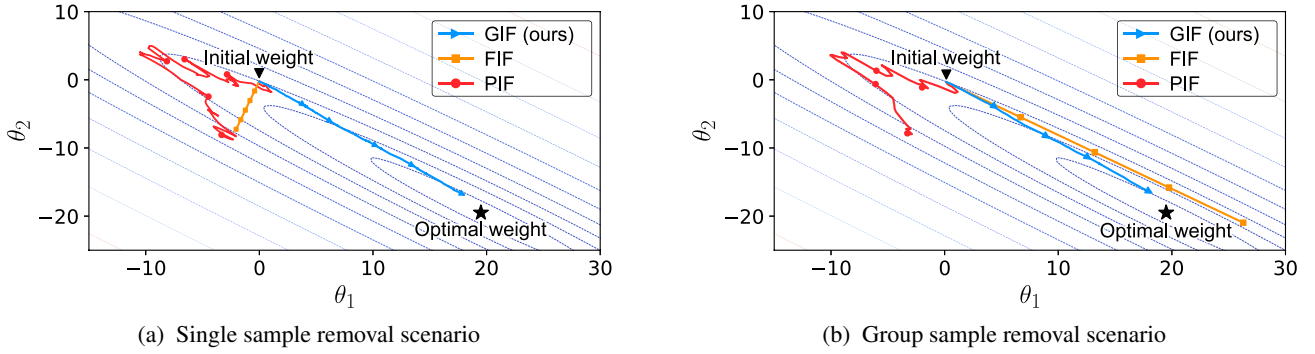


Figure 2: Visualization of MSE loss surface and three different influence functions for the linear regression model. (a) Single data point is consecutively removed 200 times. (b) The group of five data points is successively removed 40 times. The markers represent every 50th single sample removal and 10th group sample removal for each scenario. The optimal weight indicates  $(\theta_1, \theta_2)$  that provides the least mean squared error when freezing the rest parameters.

Then, the group influence function for the index set  $J$  is given by

$$\mathcal{I}(\mathbf{w}, \hat{\boldsymbol{\theta}}_J | \hat{\boldsymbol{\theta}}) = \frac{d}{d\epsilon} \hat{\boldsymbol{\theta}}_J(\epsilon, \mathbf{w}) \quad (8)$$

$$= (\mathbf{H}_{\mathbf{w}, J}^T \mathbf{H}_{\mathbf{w}, J})^{-1} \mathbf{H}_{\mathbf{w}, J}^T \left[ \sum_{i=1}^m w_i \nabla \ell(z_i, \hat{\boldsymbol{\theta}}) \right], \quad (9)$$

where  $\mathbf{H}_{\mathbf{w}, J} = [\mathbf{h}_{\mathbf{w}, j_1} | \dots | \mathbf{h}_{\mathbf{w}, j_k}]$  for  $\mathbf{H}_{\mathbf{w}, \hat{\boldsymbol{\theta}}} = [\mathbf{h}_{\mathbf{w}, 1} | \dots | \mathbf{h}_{\mathbf{w}, n}] = \sum_{i=1}^m (1 + \epsilon w_i) \nabla^2 \ell(z_i, \hat{\boldsymbol{\theta}})$ . The detailed derivation of (9) is provided in Appendix A. The effect of terms with  $\epsilon$  in  $\mathbf{H}_{\mathbf{w}, J}$  would not be negligible<sup>2</sup> when the proportion of the upweighted data is large (Koh et al. 2019; Basu, You, and Feizi 2020), whereas the  $o(\epsilon)$  term of the Hessian in (6) can be dropped. Thus, the  $\epsilon$ -involved terms should be considered to measure the influence of proportional data removal (or augmentation), which might cause a large perturbation of parameters.

## 2.4 Inspiring Example on the Linear Regression

Other forms of influence functions could be used to measure the changes in target parameters as follows:

- **Frozen IF (FIF), inspired by Guo et al. (2021)**: One viable approach involves the selective freezing of parameters  $\theta_j$ ,  $j \notin J$ . Subsequently, the original influence function can be computed using (1), treating the network as if it solely comprises parameters  $\boldsymbol{\theta}_J$ . This approach is reminiscent of Koh and Liang (2017) and Guo et al. (2021) that employed a layer-wise freezing strategy.
- **Projected IF (PIF), inspired by Schioppa et al. (2022)**: Another plausible method is to compute the influence for all parameters and then extract the  $\boldsymbol{\theta}_J$  from the influence (7). This process is equivalent to the straightforward projection from the original space to parameter space  $\hat{\boldsymbol{\theta}}_J$ . This projection is close to Schioppa et al. (2022) that adopted selection matrix, or Pruthi et al. (2020) that utilizes random projection matrix.

<sup>2</sup>However, we omit the notation of  $\epsilon$  in  $\mathbf{H}_{\mathbf{w}, J}$  and  $\mathbf{H}_{\mathbf{w}, \hat{\boldsymbol{\theta}}}$  for the brevity of notations.

Unfortunately, we find that these approaches cannot properly approximate the change direction even for the linear regression model.

**Explanatory Implementations** Figure 2 illustrates how the first two weights of the linear regression model change when the 200 heterogeneous data points are removed<sup>3</sup>. The other three weights and the bias are supposed to be fixed to observe the effect on the partial influence of the data removal. The weights are properly updated to the near-optimal by the GIF, but none of the cases are for the FIF and PIF. The FIF and PIF result in similar updated weights in Fig. 2a, but the PIF exhibits significant weight trajectory fluctuations in both removal scenarios. The FIF excessively extrapolates the influence in Fig. 2b, making a significant gap between the optimal and updated weight points.

These misdirected updates are mathematically inevitable in the FIF and PIF schemes. The derivative of FIF can be represented as

$$0 \approx \epsilon \nabla_{\boldsymbol{\theta}_J} \ell(z, \hat{\boldsymbol{\theta}}) + \begin{bmatrix} \mathbf{H}_{J \times J} & \mathbf{0} \\ \mathbf{0} & \mathbf{0} \end{bmatrix} \begin{bmatrix} \Delta \epsilon \\ \mathbf{0} \end{bmatrix}, \quad (10)$$

where  $\mathbf{H}_{J \times J} \in \mathbb{R}^{k \times k}$ . The matrix  $\mathbf{H}_{J \times J}$  is essentially  $\mathbf{H}_J$  with all rows where the index  $j > k$  are eliminated. As a consequence, the loss of information within the gradients and Hessians leads to misdirected updates.

The PIF generates the wrong update direction because matrix  $\mathbf{H}_{\hat{\boldsymbol{\theta}}}$  is non-orthogonal. We note that  $\mathbf{H}_J (\mathbf{H}_J^T \mathbf{H}_J)^{-1} \mathbf{H}_J^T$  is a projection matrix, then  $\mathcal{I}(z, \hat{\boldsymbol{\theta}}_J | \hat{\boldsymbol{\theta}})$  can be considered as projection coefficients. Then, the PIF attempts to use the coefficients from another space (column space of  $\mathbf{H}$ ) to properly project  $\nabla \ell(z, \hat{\boldsymbol{\theta}})$  onto the column space of  $\mathbf{H}_J$ . This only works when  $\mathbf{H}$  is orthogonal, which is rarely the case.

<sup>3</sup>1000 data points are artificially manipulated by a linear mapping from  $\mathbb{R}^5$  to  $\mathbb{R}$  with noise from the standard normal distribution. 20% of data points are given heterogeneous properties by amplifying and flipping their sizes and signs, respectively.

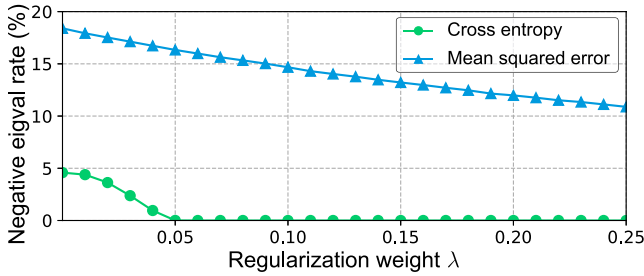


Figure 3: Percentage of negative eigenvalue vs.  $L_2$  regularization weight  $\lambda$  for the MNIST classification task on the fully-connected network. Eigenvalues are computed by using the Lanczos algorithm (Lanczos 1950).

### 3 Numerical Approximation of GIF

The GIF can reduce the required computations by excluding the computation of  $\mathbf{H}_{-J}$ . This feature proves particularly efficient when  $\mathbf{H}_J$  is significantly smaller than  $\mathbf{H}_{-J}$ , especially in large-scale networks. However, the existing algorithm to approximate inverse-Hessian-vector product cannot be directly employed for GIFs and large networks. The algorithm necessitates strong convexity and tends to be unstable in large networks (Basu, Pope, and Feizi 2021). We tailor a new algorithm for the GIFs, which does not require any specific configurations on the networks.

#### 3.1 Existing Algorithm to Approximate IF

Koh and Liang (2017); Basu, You, and Feizi (2020) propose an iterative method that can approximately compute inverse-Hessian-vector product by using the Neuman series (Stewart 2001), Hessian-vector product (Pearlmutter 1994), and stochastic Hessian-estimator (Agarwal, Bullins, and Hazan 2017). The iterative approximation can be represented as

$$\mathcal{I}_k = \mathcal{I}_0 + (\mathbf{I} - \mathbf{H}_{\hat{\theta}})\mathcal{I}_{k-1}, \quad (11)$$

where  $\mathcal{I}_0 = \nabla \ell(z, \hat{\theta})$  and  $\mathbf{H}_{\hat{\theta}}$  is estimated from  $\nabla^2 \ell(z_{s_t}, \hat{\theta})$  for uniformly chosen  $t$  data samples  $z_{s_1}, \dots, z_{s_t}$ .

This recursive series converges as  $\mathcal{I}_k \rightarrow \mathcal{I}(z, \hat{\theta})$  as  $k \rightarrow \infty$  only if the spectral radius<sup>4</sup> of  $\mathbf{I} - \mathbf{H}_{\hat{\theta}}$  is less than 1. In other words, all eigenvalues of the estimated Hessian must be within  $[0, 1)$ , which is hardly the case<sup>5</sup>. To mitigate the spectral radius condition, Koh et al. (2019); Basu, You, and Feizi (2020) adopt  $L_2$ -regularization (or damper) term and scale the loss down to avoid the divergence of the series.

Nonetheless,  $L_2$ -regularization still cannot be a master key for the convergence of the series (11). Figure 3 shows the percentage of negative eigenvalues among the top 500 eigenvalues with the largest absolute values in the Hessian matrix, obtained from the Lanczos algorithm. The negative eigenvalue rate for the cross-entropy implies that the Hessian matrix is positive semi-definite for large enough  $\lambda$ . However,

<sup>4</sup>The spectral radius of matrix  $\mathbf{A} \in \mathbb{R}^{n \times n}$  is defined as  $\rho(\mathbf{A}) = \max\{|\lambda_1|, \dots, |\lambda_n|\}$ , where  $\lambda_1, \dots, \lambda_n$  are the eigenvalues of  $\mathbf{A}$ .

<sup>5</sup>Theoretically, convex loss functions can meet the condition, but non-convexity is prevalent in modern AI models.

there is no way to pre-determine the proper  $\lambda$  for a given network. Moreover, such  $\lambda$  may exist outside of the viable range as in the case of the mean squared error.

#### 3.2 Robust and Efficient GIF Approximation

We introduce a plug-and-play algorithm that can be applied to any network by utilizing the positive definiteness and scale-invariance of the GIF. The series (11) can be simply extended to the case of GIF as

$$\mathcal{I}_k = \mathcal{I}_0 + (\mathbf{I} - \mathbf{H}_J^T \mathbf{H}_J) \mathcal{I}_{k-1} \quad (12)$$

and  $\mathcal{I}_0 = \mathbf{H}_J^T \nabla \ell(z, \hat{\theta})$ . Similar to (11), the spectral radius of  $\mathbf{I} - \mathbf{H}_J^T \mathbf{H}_J$  should be less than 1 for the series (12) to converge. Unfortunately, the series often diverges in real implementation even in the convex loss function, due to the subtle perturbations in numerical computations. Divergence of the fast IF approximation algorithm (11) is a major obstacle that postpones the Renaissance of network analysis via IF.

We find that the GIF can detour the divergence issue for any network and loss function. Though the series can diverge, Prop. 1 guarantees that a substitutive loss and empirical risk, (12) of which stably converges, can be utilized to compute the series of the original network.

**Proposition 1.** *For any  $\ell(\cdot)$  and  $\mathcal{L}(\cdot)$ , the following arguments hold:*

- i) *The GIF is scale-invariant. i.e., scalar multiplication on the loss  $\ell(\cdot)$  and empirical risk  $\mathcal{L}(\cdot)$  does not affect the GIF.*
- ii) *There always exists  $M > 0$  such that the series (12) for the  $\frac{1}{M}\ell(\cdot)$  and  $\frac{1}{M}\mathcal{L}(\cdot)$  converges.*

*Proof.* See Appendix B. □

Proposition 1 is useful, especially in real implementations. All we need to do is just divide the loss by some large  $M$  only when the code for computing the IF is executed.

Moreover, we can avoid the direct  $\mathcal{O}(n^3)$  computation of  $\mathbf{H}_J^T \mathbf{H}_J$  by cleverly applying HVP. Note that  $\mathbf{H}_J^T \mathbf{H}_J$  is the  $k \times k$  leading principal submatrix of  $\mathbf{H}^T \mathbf{H}$ , so the following equality holds for  $v \in \mathbb{R}^k$ :

$$\mathbf{H}^T \mathbf{H} \begin{bmatrix} v \\ \mathbf{0} \end{bmatrix} = \begin{bmatrix} \mathbf{H}_J^T \\ \mathbf{H}_{-J}^T \end{bmatrix} [\mathbf{H}_J | \mathbf{H}_{-J}] \begin{bmatrix} v \\ \mathbf{0} \end{bmatrix} = \begin{bmatrix} \mathbf{H}_J^T \mathbf{H}_J v \\ \mathbf{H}_J^T \mathbf{H}_{-J} v \end{bmatrix}. \quad (13)$$

Therefore, the series in Prop. 1 can be computed by applying the HVP twice, which takes the same complexity  $\mathcal{O}(n)$  as the original IF.

### 4 Finding Good Combinations of Parameters

Classifying highly relevant parameter  $\theta_J$  is crucial to optimize the utility after modifying the network. However, computing the GIF for every possible  $J$  is infeasible even for a very simple network. The number of combinations for choosing 100 parameters out of one thousand parameters ( $\approx 10^{140}$ ) outstrips the number of atoms in the universe ( $\approx 10^{82}$ ). We propose empirical parameter selection methods to detour the combinatorial explosion, inspired by the neurological approach that analyzes how the specific areas of the brain respond to certain tasks or stimuli (Penny et al. 2011).

---

**Algorithm 1:** Numerical implementation of the group GIF

---

**Input** model parameter  $\hat{\theta}$ , loss  $\ell$ , set of data  $z_1, \dots, z_m \in Z$ , indicator  $\mathbf{w} = [w_1, \dots, w_m]^T \in \{1, 0\}^m$ .

1:  $\mathcal{L}(\hat{\theta}) \leftarrow \sum_{i=1}^m \ell(z_i, \hat{\theta})$ ,  $\mathcal{L}_{\mathbf{w}}(\hat{\theta}) \leftarrow \sum_{i=1}^m w_i \ell(z_i, \hat{\theta})$ .

2: Determine parameter set  $J$  when computing  $\mathcal{L}_{\mathbf{w}}(\hat{\theta})$ .

3:  $\mathcal{I}(z, \hat{\theta}_J | \hat{\theta}) \leftarrow$  Compute the series (12) until it converges.

**Return**  $\mathcal{I}(z, \hat{\theta}_J | \hat{\theta})$

---

We are also motivated by selection mechanisms of the pruning and quantization of neural networks. While the selection methods for the GIF target to choose the most relevant parameters, the pruning methods aim to remove the least important connections to compress the network. Hu et al. (2016) suggested a trimming method to get rid of zero activations, and Lee, Ajanthan, and Torr (2019); Wang, Zhang, and Grosse (2020) proposed pruning methods by utilizing the gradient of the network.

**Parameter selection criteria** We design two criteria that select highly active neurons during the feed-forward and feedback process, so-called Top- $k$  outputs and Top- $k$  gradients. These criteria are compared with two benchmarks: threshold and random criteria. Specifically, the four criteria select network parameters from a given layer as follows:

- **Top- $k$  outputs** selects  $k$  parameters that generate the outputs higher than the other outputs.
- **Top- $k$  gradients** chooses  $k$  parameters that associate with the gradient outputs higher than the other gradient outputs.
- **Threshold** randomly picks  $k$  parameters that associate with the layer outputs higher than the given threshold.
- **Random** literally selects  $k$  parameters randomly.

The number of selected parameters  $k$  is determined proportional to the number of parameters for each layer. These selection methods are implemented as callback functions that are executed when each layer is called during the feed-forward or back-propagation. Then, the parameter selection can be processed without adding selection stages.

A plug-and-play GIF algorithm<sup>6</sup> can be devised by combining the numerical series (12) and the parameter selection method, as in Alg. 1. The GIF for a single data point can be computed by defining the indicator vector  $\mathbf{w}$  as a one-hot vector. Once  $\mathcal{L}(\hat{\theta})$ ,  $\mathcal{L}_{\mathbf{w}}(\hat{\theta})$  and  $J$  are given, the series (12) can be computed by using the hessian vector-product.

## 5 Numerical Implementations

We measure the effect of the GIF to answer the following questions:

- How does the network change according to the selection of the parameters?
- Does the GIF effectively update the network, compared with alternative methods?

---

<sup>6</sup>Pythonic programmable pseudo-code is provided in Appendix.

Table 1: Update results for the four selection criteria. Cross-entropy losses are computed on ResNet-18 with the MNIST dataset.

Criteria	Loss	Modification Ratio (MR%)			
		5	10	30	50
Top- $k$ outputs	Self-loss $\uparrow$	6.23	6.21	<b>5.13</b>	4.89
	Test loss $\downarrow$	<u>0.05</u>	<b>0.11</b>	<b>0.64</b>	<b>0.69</b>
Top- $k$ gradients	Self-loss $\uparrow$	<b>6.24</b>	<b>6.29</b>	4.95	<b>4.89</b>
	Test loss $\downarrow$	<b>0.04</b>	<u>0.12</u>	1.02	0.81
Threshold	Self-loss $\uparrow$	4.42	4.81	3.71	4.33
	Test loss $\downarrow$	0.09	0.65	1.78	1.18
Random	Self-loss $\uparrow$	4.42	4.79	3.36	4.26
	Test loss $\downarrow$	0.08	0.60	2.63	1.46

\*Best: **bold**, second-best: underline.

- Do the updates change the parameters uniformly across the entire network?

We utilize ResNet-18 (He et al. 2016) and VGG-11 (Simonyan and Zisserman 2015) networks; and MNIST (Lecun et al. 1998) and CIFAR-10 (Krizhevsky and Hinton 2009) datasets on our implementations. All experiments are conducted on the Linux workstation with AMD Ryzen<sup>TM</sup>7 5800X 8-Core Processor CPU @ 3.70GHz and one NVIDIA Geforce RTX 3090 GPU.

**Experiment setups** We apply the GIF to three trained networks: 1) ResNet-18 with MNIST dataset, 2) VGG-11 with CIFAR-10 dataset, and 3) our custom convolutional neural network with backdoor MNIST dataset. The experimental configurations to generate the presented results are described in Appendix C.

**Data sampling** We sample the dataset twice to compute two losses; one for hessian  $\mathbf{H}_J$  and the other for gradient  $\sum_{i=1}^m w_i \nabla \ell(z_i, \hat{\theta})$ . The data sampling approach draws inspiration from second-order Hessian computation (Agarwal, Bullins, and Hazan 2017) and is in line with the research on the acceleration of influence functions (Guo et al. 2021).

**Evaluation metrics** We define self and test loss to measure the effect of the GIF. The self-loss indicates  $\mathcal{L}_{\mathbf{w}}(\hat{\theta})$  in Alg. 1, the loss for the target dataset where the influence is measured. Meanwhile, the test loss indicates the loss for the test dataset. However, for the class removal task, we measure the test loss after eliminating data from the test dataset when the data belongs to the removed class. The self and test accuracy metrics are measured in the same way as the losses are measured.

### 5.1 The Effects of Parameter Selection Criteria

We conduct a data removal from the ResNet-18 trained from the MNIST dataset to measure the effects of the four selection criteria. Data with label “8” is removed from the network by using Alg. 1. We define the modification ratio (MR%) as the ratio between the number of updated and total parameters.

We empirically multiply scalar values to the influence function to find the optimal network utility. The (MR%, scalar

Table 2: Numerical comparisons for three influence functions on the VGG-11 network trained by CIFAR-10 dataset. Numbers with the percentage (10%, 30%, and 50%) are the MR%. The average time implies the elapsed time to compute one iteration of the series (12).

Methods	Avg. time (ms)	Test acc. (%) $\uparrow$			Test loss $\downarrow$			Self-acc. (%) $\downarrow$			Self-loss $\uparrow$			$F_1$ score $\uparrow$		
		10 %	30 %	50 %	10 %	30 %	50 %	10 %	30 %	50 %	10 %	30 %	50 %	10 %	30 %	50 %
GIF (ours)	<b>522</b>	<b>86.40</b>	<b>83.59</b>	<b>76.62</b>	<b>0.51</b>	<b>0.60</b>	<b>1.98</b>	<b>0.43</b>	<b>3.10</b>	<b>5.03</b>	<b>6.135</b>	<b>7.29</b>	<b>6.89</b>	<b>0.93</b>	<b>0.90</b>	<b>0.85</b>
FIF (Guo et al. 2021)	529	85.16	77.42	70.99	0.60	0.97	1.36	1.73	5.95	7.23	6.129	6.80	6.26	0.91	0.85	0.80
PIF (Schioppa et al. 2022)	546	63.53	66.21	62.76	1.98	1.82	1.98	14.76	18.21	12.56	5.09	4.91	5.39	0.73	0.73	0.73
Retraining	-	91.34			0.36			0			9.85			0.95		

\*Best: **bold**.

value) pairs used to generate Table 1 are (5, 150), (10, 95), (30, 85), (50, 28).

**Results** Table 1 describes the results of the class removal tasks for each selection criteria. We observe that the two top- $k$  methods outperform the two naive approaches, which implies that there might exist winning tickets in the parameter combination lottery, as in the case of network pruning (Frankle and Carbin 2019). The top- $k$  outputs criterion shows comparable losses to top- $k$  gradients when the MR% is low ( $\leq 10$ ), but the top- $k$  outputs criterion outperforms the top- $k$  gradients as the MR% increases.

Interestingly, the updated network has a better loss value when the modification rate is low in all cases. This result may imply that the fragility of the influence function comes from the inordinate modifications. This phenomenon is not transient, and we observe similar results across the experiments.

## 5.2 Comparison to Alternative Influence Functions

We evaluate the losses and accuracies of the GIF, extending the linear regression with synthetic data points in Fig. 2. We conduct a class removal task on the VGG-11 with the CIFAR-10 dataset and remove all “ship” images from the training dataset. The FIF and PIF, the freezing and projection methods, are adopted as baselines in Fig. 2. We first select the {10, 30, 50}% of parameters from the network by using the Top- $k$  outputs criterion, then update the parameters according to the approximation results of the GIF, FIF, and PIF.

In principle, the FIF and PIF should be computed by the original inverse-hessian approximation (11) to exactly evaluate the proposed approaches. However, we apply the newly defined series (12) due to the instability of the original approximation algorithm.

Similar to Sec. 5.1, different scalar multiplications are applied for each MR% and the evaluated algorithms. For a fair comparison between different scales, we adopt a modified  $F_1$  score to harmonically maximize the test accuracy and  $1 - \text{self-accuracy}$ . Thus, the modified  $F_1$  score is computed as

$$F_1 = 2 \times \frac{(1 - \text{self-accuracy}) \times \text{test accuracy}}{(1 - \text{self-accuracy}) + \text{test accuracy}}. \quad (14)$$

**Results** Table 2 shows the evaluation results of the three IF schemes on the VGG-11 network. The GIF outperforms the other two methods for the {self, test}-accuracy and test loss. Especially for MR% 10, the GIF well eradicates the trained

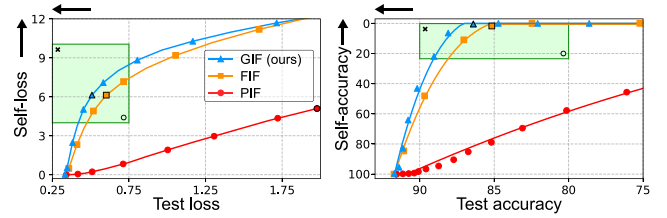


Figure 4: Loss and accuracy results of three influence schemes for various influence scales at MR% 10. The black-edged markers are the values in Table 2. The green areas and the {x, o} marks in the two graphs correspond to each other, representing desirable regions with self-accuracy lower than 20% and test accuracy higher than 80%. The arrows indicate the direction of improvements.

data from the network, closely approximating the state of the retrained network. The GIF also has a shorter computation time compared with the other methods. The FIF involves with  $\mathbf{H}_{J \times J} \in \mathbb{R}^{k \times k}$ , but numerically, additional indexing process is inevitable to parse  $\mathbf{H}_{J \times J}$  from  $\mathbf{H}_J \in \mathbb{R}^{n \times k}$ . Meanwhile, the PIF extracts the partial changes after computing the entire changes. Thus, the other two methods require extra processes to estimate the parameter changes.

Figure 4 illustrates the variations in losses and accuracies during the update process of VGG-11 using the GIF, FIF, and PIF. The influences of these three approaches are gradually amplified by an increasing scalar factor to draw discernible patterns of loss and accuracy. Regardless of the  $F_1$  score and scalar scale of the influence, the GIF consistently demonstrates superior network utility compared to the alternative schemes. Moreover, the outcomes are coherent with the findings from the linear regression experiment (Fig. 2b), in the sense that the GIF and FIF have a similar tendency, where a parallel trend is observed between GIF and FIF, while the PIF exhibits a decline in utility attributed to misdirected updates.

## 5.3 Backdoored Model Recovery

Though the GIF will preserve the model utility in the previous class removal scenario, we suspect that the successful result may come from the parameter changes in the layers close to the output layers. For example, we can manipulate one component in softmax output close to zero by just making the associated bias extremely low.

We design a backdoor (BD) scenario to examine whether

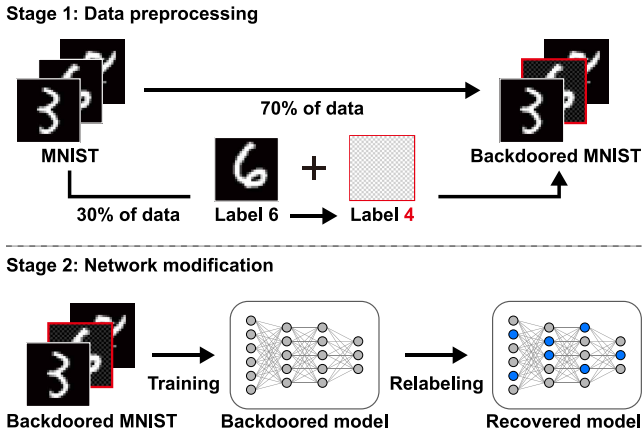


Figure 5: Backdoored model recovery scenario. In stage 1, the backdoor pattern is implanted on 30% of randomly chosen data. The labels of the data are changed into “4” either. In stage 2, the backdoored model is trained by the backdoored MNIST dataset, then recovered by the GIF in the relabeling process. The contrast of the backdoor pattern in this figure is exaggerated threefold for visibility.

the GIFs appropriately modify the network parameters, as in Fig. 5. We train a BD model with BD MNIST processed by stage 1. The trained model returns a BD label for given BD data, but it normally operates when non-BD data is given. If the model is properly recovered by the GIF (stage 2), the model should provide proper outputs for both BD and non-BD data. Our custom neural network is utilized as a BD model, which consists of four convolutional layers and one fully-connected layer.

**Results** Table 3 lists the accuracy of the models in the BD scenario. One interesting point is that the test accuracies of the relabel task are higher than those of the class removal task even though the number of BD data is almost three times higher than the number of removed data. These results indicate that the recovered model in the BD task recycles the selected parameters rather than removes the effect of the parameters.

Remarkably, the GIF achieves the test accuracy of the re-trained model by just conducting one-shot modification for 10% of parameters. There is an accuracy gap between the modified and retrained models when we evaluate the recovered model with the BD data with true labels, but this gap is inevitable because the retrained model utilizes the BD data with true labels as training data. These results cannot be obtained if the parameter changes occur adjacent to the output layer, as the GIF should recognize parameters associated with the backdoor patterns and properly modify the parameters. The results imply that the GIF can robustly predict the network change while well preserving the network utility.

#### 5.4 How Does the Number of Target Parameters Changes the Network Utility?

The numerical results empirically confirm that the over-ly-chosen target parameters can indeed deteriorate the network

Table 3: Accuracy (%) of models for given data and labels. MR% {10, 30, 50} implies the model where {10, 30, 50}% of parameters are updated by the GIF.

Method	BD data w/ BD label	BD data w/ true label	Test dataset
BD Model	100.00	9.50	98.96
MR% 10	9.52	98.63	98.46
MR% 30	9.64	97.49	98.33
MR% 50	9.72	91.57	86.48
Retraining	9.46	99.76	98.98

utility. These outcomes are coherent with our earlier conjecture, wherein the incremental nuisance changes in irrelevant parameters might accumulate within the network. In Table 1, the self-losses in Top- $k$  outputs, gradients show a significant 21.5% reduction as the MR% increases from 5 to 50. Conversely, the Threshold and Random criteria merely yield 3.5% self-loss declines because they fail to effectively select suitable parameters. Parallel outcomes can be consistently observed in Table 2 and 3, where network utility is maximized only when an appropriate number of parameters is judiciously chosen.

## 6 Discussion

We have discussed the effect of data on a set of parameters in the network. The GIF shows noteworthy results on both class removal and backdoor recovery tasks. With the robust inverse Hessian approximation and streamlined parameter selection criteria, the GIF facilitates the adoption of influence functions as analytical tools. However, limitations of the GIF have also been noted.

**Limitations and Future works** Ideally, influence functions should count all parameter changes. However, our approaches intentionally restrict changes in the non-selected parameters, based on our conjecture that the changes in some parameters can deteriorate network utilities. A deeper theoretical analysis might provide improved influence approximations, getting close to the ideal influence functions.

Another important but unresolved problem is finding the combinatorial optimum of the parameters. We confirm that a sweet spot exists in the combination of the hyper-parameters such as target parameters, modification ratio, scalar influence scales, and sampled data. However, finding the rule of thumb for these configurations is quite challenging.

Continued research will focus on enhancing the efficiency of GIFs, as well as gaining a comprehensive understanding of the nature of their hyper-parameters. This endeavor aims to provide us with complete accessibility to AI models.

## References

Agarwal, N.; Bullins, B.; and Hazan, E. 2017. Second-Order Stochastic Optimization for Machine Learning in Linear Time. *Journal of Machine Learning Research*, 18(116): 1–40.

- Anderson, M. 2023. ‘AI Pause’ Open Letter Stokes Fear and Controversy. *IEEE Spectrum*.
- Bae, J.; Ng, N. H.; Lo, A.; Ghassemi, M.; and Grosse, R. B. 2022. If Influence Functions are the Answer, Then What is the Question? In *Proceedings of the 36th International Conference on Neural Information Processing Systems*.
- Barredo Arrieta, A.; Díaz-Rodríguez, N.; Del Ser, J.; Bennetot, A.; Tabik, S.; Barbado, A.; Garcia, S.; Gil-Lopez, S.; Molina, D.; Benjamins, R.; Chatila, R.; and Herrera, F. 2020. Explainable Artificial Intelligence (XAI): Concepts, taxonomies, opportunities and challenges toward responsible AI. *Information Fusion*, 58: 82–115.
- Basu, S.; Pope, P. E.; and Feizi, S. 2021. Influence Functions in Deep Learning Are Fragile. In *Proceedings of the 9th International Conference on Learning Representations*.
- Basu, S.; You, X.; and Feizi, S. 2020. On Second-Order Group Influence Functions for Black-box Predictions. In *Proceedings of the 37th International Conference on Machine Learning*, 715–724.
- Bau, D.; Zhu, J.-Y.; Strobel, H.; Lapedriza, A.; Zhou, B.; and Torralba, A. 2020. Understanding the Role of Individual Units in a Deep Neural Network. *Proceedings of the National Academy of Sciences*, 117(48): 30071–30078.
- Brunet, M.-E.; Alkalay-Houlihan, C.; Anderson, A.; and Zemel, R. 2019. Understanding the Origins of Bias in Word Embeddings. In *Proceedings of the 36th International Conference on Machine Learning*, 803–811.
- Cohen, G.; and Giryas, R. 2022. Membership Inference Attack Using Self Influence Functions. arXiv:2205.13680.
- Emerson, R. W. 1841. *Self-Reliance*, 79–116. Project Gutenberg.
- Epifano, J. R.; Ramachandran, R. P.; Masino, A. J.; and Rasool, G. 2023. Revisiting the Fragility of Influence Functions. *Neural Networks*, 162: 581–588.
- Frankle, J.; and Carbin, M. 2019. The Lottery Ticket Hypothesis: Finding Sparse, Trainable Neural Networks. In *Proceedings of the 7th International Conference on Learning Representations*.
- Guo, H.; Rajani, N.; Hase, P.; Bansal, M.; and Xiong, C. 2021. FastIF: Scalable Influence Functions for Efficient Model Interpretation and Debugging. In *Proceedings of the 2021 Conference on Empirical Methods in Natural Language Processing*, 10333–10350.
- Hampel, F. R. 1974. The Influence Curve and Its Role in Robust Estimation. *Journal of the American Statistical Association*, 69(346): 383–393.
- He, K.; Zhang, X.; Ren, S.; and Sun, J. 2016. Deep Residual Learning for Image Recognition. In *Proceedings of 2016 IEEE/CVF Conference on Computer Vision and Pattern Recognition*, 770–778.
- Hu, H.; Peng, R.; Tai, Y.; and Tang, C. 2016. Network Trimming: A Data-Driven Neuron Pruning Approach towards Efficient Deep Architectures. *CoRR*, abs/1607.03250.
- Jain, S.; Manjunatha, V.; Wallace, B.; and Nenkova, A. 2022. Influence Functions for Sequence Tagging Models. In *Proceedings of the 2022 Conference on Empirical Methods in Natural Language Processing*, 824–839.
- Koh, P. W.; Ang, K.-S.; Teo, H. H. K.; and Liang, P. 2019. On the Accuracy of Influence Functions for Measuring Group Effects. In *Proceedings of the 33rd International Conference on Neural Information Processing Systems*, 5254–5264.
- Koh, P. W.; and Liang, P. 2017. Understanding Black-box Predictions via Influence Functions. In *Proceedings of the 34th International Conference on Machine Learning*, 1885–1894.
- Koh, P. W.; Steinhardt, J.; and Liang, P. 2022. Stronger Data Poisoning Attacks Break Data Sanitization Defenses. *Machine Learning*, 111(1): 1–47.
- Kong, S.; Shen, Y.; and Huang, L. 2022. Resolving Training Biases via Influence-based Data Relabeling. In *Proceedings of the 10th International Conference on Learning Representations*.
- Krizhevsky, A.; and Hinton, G. 2009. Learning Multiple Layers of Features from Tiny Images. *Master’s thesis, Department of Computer Science, University of Toronto*.
- Lanczos, C. 1950. An Iteration Method for the Solution of the Eigenvalue Problem of Linear Differential and Integral Operators. *Journal of research of the National Bureau of Standards*, 45: 255–282.
- Lecun, Y.; Bottou, L.; Bengio, Y.; and Haffner, P. 1998. Gradient-Based Learning Applied to Document Recognition. *Proceedings of the IEEE*, 86(11): 2278–2324.
- Lee, D.; Park, H.; Pham, T.; and Yoo, C. D. 2020. Learning Augmentation Network via Influence Functions. In *Proceedings of the IEEE/CVF Conference on Computer Vision and Pattern Recognition*.
- Lee, N.; Ajanthan, T.; and Torr, P. H. 2019. SNIP: Single-Shot Network Pruning Based on Connection Sensitivity. In *Proceedings of the 7th International Conference on Learning Representations*.
- Olah, C.; Satyanarayan, A.; Johnson, I.; Carter, S.; Schubert, L.; Ye, K.; and Mordvintsev, A. 2018. The Building Blocks of Interpretability. *Distill*. <https://distill.pub/2018/building-blocks>.
- Pearlmutter, B. A. 1994. Fast Exact Multiplication by the Hessian. *Neural Computation*, 6(1): 147–160.
- Penny, W. D.; Friston, K. J.; Ashburner, J. T.; Kiebel, S. J.; and Nichols, T. E. 2011. *Statistical Parametric Mapping: the Analysis of Functional Brain Images*. Academic Press.
- Pruthi, G.; Liu, F.; Kale, S.; and Sundararajan, M. 2020. Estimating Training Data Influence by Tracing Gradient Descent. In *Proceedings of the 34th International Conference on Neural Information Processing Systems*, 19920–19930.
- Schioppa, A.; Zablotskaia, P.; Vilar, D.; and Sokolov, A. 2022. Scaling Up Influence Functions. In *Proceedings of the AAI Conference on Artificial Intelligence*, volume 36, 8179–8186.
- Schulam, P.; and Saria, S. 2019. Can You Trust This Prediction? Auditing Pointwise Reliability After Learning. In *Proceedings of the 22nd International Conference on Artificial Intelligence and Statistics*, 1022–1031.
- Simonyan, K.; and Zisserman, A. 2015. Very Deep Convolutional Networks for Large-Scale Image Recognition. In *Proceedings of the 3rd International Conference on Learning Representations*.
- Stewart, G. W. 2001. *Matrix algorithms*. Society for Industrial and Applied Mathematics.
- Wang, C.; Zhang, G.; and Grosse, R. 2020. Picking Winning Tickets Before Training by Preserving Gradient Flow. In *Proceedings of the 8th International Conference on Learning Representations*.
- Wang, Z.; Zhu, H.; Dong, Z.; He, X.; and Huang, S.-L. 2020. Less Is Better: Unweighted Data Subsampling via Influence Function. In *Proceedings of the AAI Conference on Artificial Intelligence*.
- Ye, J.; Gao, J.; Wu, Z.; Feng, J.; Yu, T.; and Kong, L. 2022. ProGen: Progressive Zero-shot Dataset Generation via In-context Feedback. In *Proceedings of the 2022 Conference on Empirical Methods in Natural Language Processing*, 3671–3683.



## A Derivation of Group Generalized Influence Function

Let  $\hat{\theta}(\epsilon, \mathbf{w})$  be a minimizer of  $\mathcal{L}(\theta) + \sum_{i=1}^m w_i \ell(z_i, \theta)$ . Then, the first-order optimality condition on the empirical risk gives

$$0 \approx \nabla \mathcal{L}(\hat{\theta}(\epsilon, \mathbf{w})) + \epsilon \sum_{i=1}^m w_i \nabla \ell(z_i, \hat{\theta}(\epsilon, \mathbf{w})). \quad (15)$$

The first-order Taylor expansion of (15) anchored on  $\hat{\theta} = \operatorname{argmin}_{\theta \in \Theta} \mathcal{L}(\theta)$ , is

$$0 \approx \nabla \mathcal{L}(\hat{\theta}) + \nabla^2 \mathcal{L}(\hat{\theta}) \Delta_{\epsilon, \mathbf{w}} \quad (16)$$

$$+ \epsilon \sum_{i=1}^m w_i \nabla \ell(z_i, \hat{\theta}) + \epsilon \sum_{i=1}^m w_i \nabla^2 \ell(z_i, \hat{\theta}) \Delta_{\epsilon, \mathbf{w}} \quad (17)$$

$$= \epsilon \sum_{i=1}^m w_i \nabla \ell(z_i, \hat{\theta}) + \sum_{i=1}^m (1 + \epsilon w_i) \nabla^2 \ell(z_i, \hat{\theta}) \Delta_{\epsilon, \mathbf{w}}. \quad (18)$$

The first-order optimality also gives  $\nabla \mathcal{L}(\hat{\theta}) \approx 0$  as  $\hat{\theta}$  is a minimizer of  $\mathcal{L}(\cdot)$ . Similar to (3)-(5), the group GIF can be driven as (9).

## B Proof of Proposition 1

We first show the scale-invariance of the GIF. For  $M > 0$ , we define the downscaled loss function and empirical risk as  $\frac{1}{M} \ell(z, \hat{\theta})$  and  $\frac{1}{M} \mathcal{L}(\hat{\theta})$ . For a given index set  $J$ , the GIF of the newly-defined empirical risk is represented as

$$\left( \frac{1}{M} \mathbf{H}_J^\top \frac{1}{M} \mathbf{H}_J \right)^{-1} \frac{1}{M} \mathbf{H}_J^\top \frac{1}{M} \nabla \ell(z, \hat{\theta}) \quad (19)$$

$$= (\mathbf{H}_J^\top \mathbf{H}_J)^{-1} \mathbf{H}_J^\top \nabla \ell(z, \hat{\theta}) = \mathcal{I}(z, \hat{\theta}_J | \hat{\theta}). \quad (20)$$

Thus, the influence function is scale-invariant on the empirical risk.

We prove the second argument in Prop. 1 by showing that  $\frac{1}{M^2} \mathbf{H}_J^\top \mathbf{H}_J$  is positive definite with a sufficiently small spectral radius. Note that the eigenvalues of  $\mathbf{H}_J^\top \mathbf{H}_J$  are positive, because  $\lambda v^\top v = v^\top \mathbf{H}_J^\top \mathbf{H}_J v = \|\mathbf{H}_J v\|_2^2 \geq 0$  for any eigenvalue  $\lambda$  and eigenvector  $v$ , which implies  $\rho(\mathbf{I} - \mathbf{H}_J^\top \mathbf{H}_J) < 1$ .

Let  $M = (\rho(\mathbf{H}_J^\top \mathbf{H}_J) + 1)^{\frac{1}{2}}$ , where  $\rho(\cdot)$  is the spectral radius of the given matrix. The spectral radius of  $\frac{1}{M^2} \mathbf{H}_J^\top \mathbf{H}_J$  is

$$\rho \left( \frac{1}{M^2} \mathbf{H}_J^\top \mathbf{H}_J \right) = \frac{\rho(\mathbf{H}_J^\top \mathbf{H}_J)}{\rho(\mathbf{H}_J^\top \mathbf{H}_J) + 1} < 1. \quad (21)$$

This implies  $\rho(\mathbf{I} - \mathbf{H}_J^\top \mathbf{H}_J) > 0$ .

The Neumann series  $(\mathbf{H}_J^\top \mathbf{H}_J)^{-1} = \sum_{i=0}^{\infty} (\mathbf{I} - \mathbf{H}_J^\top \mathbf{H}_J)^i$  converges because  $\rho(\mathbf{I} - \mathbf{H}_J^\top \mathbf{H}_J) \in (0, 1)$ .

## C Experimental Details for Reproduction

### C.1 Network preparation

**ResNet-18 with MNIST dataset** We adopted ResNet-18 to produce the results in Table 1. The model is trained using the stochastic gradient descent (SGD) optimizer, with the initial learning rate  $1 \cdot 10^{-1}$ , momentum of 0.9, and weight decay of  $5.0 \cdot 10^{-4}$ . We adopt a cross-entropy loss and batch size of 256. The MNIST dataset is normalized with  $\mu = 0.1307$  and  $\sigma = 0.3081$ . The models are trained for 50 epochs (ResNet-18) and 20 epochs (our custom CNN). The learning rate is scheduled by a cosine annealing scheduler with a maximum iteration of 200 (ResNet-18). After training, the validation accuracy is 99.23%.

**Custom CNN with MNIST dataset** We used the same configurations for Table. 3, except for the scheduler and MNIST data preparation. 30% of data is sampled by using `numpy.choice(\cdot)` method with seed 1. The 30% of data, so-called BD data, is implanted check-pattern array that alters 0 and 16. To prevent overflow of MNIST data formatted by `uint8`, we clipped the implanted image array elements into `[0, 255]`. The learning rate is scheduled by a step scheduler that reduces the learning rate by a factor of 0.1 at the 10th and 15th epochs (our custom CNN). We use two CNNs: one CNN is trained with BD data and BD label, and the other is trained with BD data and original label. After training, the validation accuracy is 98.96% and 98.98%, respectively.

**VGG-10 with CIFAR-10 dataset** We adopted the same setting as ResNet-10, except for the data preparation. The CIFAR-10 is normalized as  $\mu = (0.4914, 0.4822, 0.4465)$  and  $\sigma = (0.2023, 0.1994, 0.2010)$ . After training, the validation accuracy is 91.93%.

## D Pythonic Implementation of Alg. 1

Variables in the `compute_GIF(·)` are matched with Alg. 1 as follows: `total_loss` for  $\mathcal{L}(\hat{\theta})$ ; `target_loss` for  $\mathcal{L}_w(\hat{\theta})$ ; `parser` for the selection criterion; and `parameter_indices` for the parameter set  $J$ . The `parser` internally implements the `hook` function, to generate the network indices from the feed-forward (or back-propagation) stage.

Function `_GIF(·)` implements the series (12). In real implementations, computing  $\mathcal{I}_{k-1} - \mathbf{H}_J^T \mathbf{H}_J \mathcal{I}_{k-1}$  is more efficient than computing  $(I - \mathbf{H}_J^T \mathbf{H}_J) \mathcal{I}_{k-1}$ , as in lines 21-24. The hessian-vector products are applied twice to compute  $\mathbf{H}_J^T \mathbf{H}_J \mathcal{I}_{k-1}$ . One can additionally divide the two losses with some number if the series does not converge.

```
1 def compute_GIF(net, total_data, target_data):
2     total_loss = criterion(net, total_data)
3     parser = selection(net, num_param)
4     target_loss = criterion(net, target_data)
5     parameter_indices = parser.get_parameter_indices()
6
7     return _GIF(net, total_loss, target_loss, parameter_indices)
8
9 def _GIF(net, total_loss, target_loss, indices):
10     # hvp(loss, model, vector) computes the hessian-vector product
11     # grad() describes the gradient of a given loss.
12
13     # I_0 in Eq. (12).
14     v = grad(target_loss, model)
15     GIF_0 = hvp(total_loss, model, v)[indices]
16
17     # Repeat until the series (10) converges.
18     while diff > tol:
19         GIF_old = GIF_new
20         GIF_new = GIF_0 + GIF_old
21                 - hvp(total_loss,
22                       model,
23                       hvp(total_loss, model, IHVP_old)[indices]
24                         )[indices]
25         diff = torch.norm(IHVP_new - IHVP_old)
26
27     return GIF
```

Listing 1: Pythonic pseudo-code of the GIF.